

Army Research Laboratory

Aberdeen Proving Ground, MD 21005-5066

ARL-TR-2445

April 2001

Effect of Body Cross Section on Projectile Aerodynamic Performance With Application to Electromagnetic (EM) Guns

Paul Weinacht

Weapons and Materials Research Directorate, ARL

Approved for public release; distribution is unlimited.

Abstract

The most effective bore cross-section geometry for electromagnetic (EM) guns may differ significantly from the circular cross section of conventional guns. The geometry of the bore cross section will influence the shape of the armature/subprojectile launch package. For certain applications, a noncircular cross section may provide payload packaging benefits which have not been considered previously for conventional circular cross-section guns. Whether these benefits can be fully realized depends, in part, on the aerodynamic performance of these geometries in free flight. The current study considers the aerodynamics of chemical energy (CE)-type munitions to determine whether there are potential aerodynamic benefits for noncircular cross-section geometries compared with conventional circular cross-section bodies. The study compares the aerodynamic drag and static stability of both circular and noncircular geometries using sophisticated computational aerodynamic predictive tools to determine the potential aerodynamic benefits.

Contents

List of Figures	v
1. Introduction	1
2. Computational Approach	3
3. Results	4
3.1 Aerodynamics of the Baseline Circular Cross-Section Geometry	5
3.2 Comparison of Aerodynamics Between Circular and Noncircular Geometries	7
3.3 Effect of Roll Orientation on Aerodynamic Performance	13
4. Conclusion	16
5. References	17
Distribution List	19
Report Documentation Page	25

INTENTIONALLY LEFT BLANK.

List of Figures

Figure 1. Schematic illustration of the baseline circular cross-section flight body.....	2
Figure 2. Schematic illustration of the noncircular cross-section geometries.....	2
Figure 3. Development of the drag coefficient over the baseline circular cross-section geometry.....	5
Figure 4. Development of the normal force coefficient over the baseline circular cross-section geometry.....	6
Figure 5. Development of the pitching moment coefficient over the baseline circular cross-section geometry.....	7
Figure 6. Development of the drag coefficient over the baseline circular cross-section and noncircular cross-section geometries.....	8
Figure 7. Development of the drag coefficient over the noncircular cross-section geometries and equivalent cross-sectional area circular geometries.....	8
Figure 8. Development of the pitching moment coefficient over the circular cross-section geometries.....	9
Figure 9. Development of the normal force coefficient over the circular cross-section geometries.....	10
Figure 10. Development of the pitching moment coefficient over the baseline circular cross-section and noncircular cross-section geometries.....	11
Figure 11. Development of the normal force coefficient over the baseline circular cross-section and noncircular cross-section geometries.....	11
Figure 12. Crossflow particle traces at $X/D=7.5$, circular cross-section body, Mach 3, 2° angle of attack.....	12
Figure 13. Crossflow particle traces at $X/D=7.5$, 43-mm noncircular cross-section body, Mach 3, 2° angle of attack.....	12
Figure 14. Effect of roll orientation on the development of the normal force coefficient over the baseline circular cross-section geometry.....	14
Figure 15. Effect of roll orientation on the development of the pitching moment coefficient over the baseline circular cross-section geometry.....	14
Figure 16. Effect of roll orientation on the development of the normal force coefficient over the 43-mm noncircular cross-section geometry.....	15
Figure 17. Effect of roll orientation on the development of the pitching moment coefficient over the baseline circular cross-section geometry.....	15

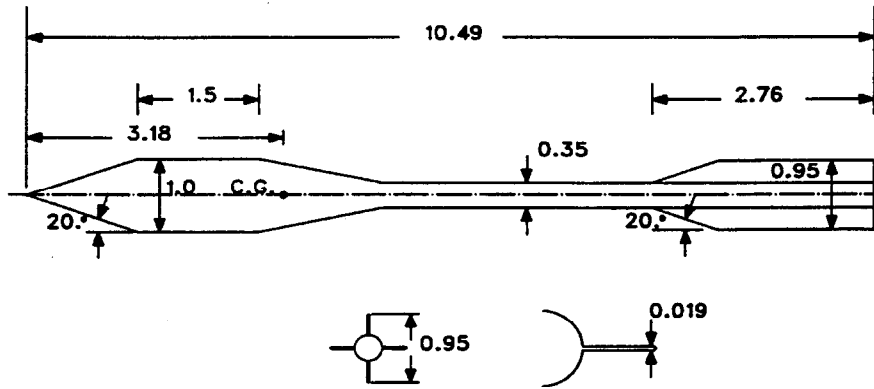
INTENTIONALLY LEFT BLANK.

1. Introduction

The U.S. Army is currently investigating electromagnetic (EM) guns as a means of increasing the lethality of its weapon systems. Currently, the geometric configuration of EM guns is a subject of research. In particular, the bore cross section of these guns may not be circular as with most conventional powder guns, but rather may possess a square or rectangular cross section. The geometry of the bore cross section will directly influence the shape of the armature/subprojectile launch package. For certain applications, the noncircular cross section may provide payload packaging benefits which have not been considered previously for conventional circular cross-section guns. Whether these benefits can be fully realized depends on a number of factors. One of the considerations is the aerodynamic performance of these geometries in free flight.

The current study considers the aerodynamics of chemical energy (CE)-type munitions to determine whether there are potential aerodynamic benefits for noncircular cross-section geometries compared with conventional circular cross-section bodies. For instance, it may be possible to package explosively formed projectile (EFP) warheads more effectively in a noncircular geometry than in a conventional circular geometry. The study compares the aerodynamic drag and static stability of both circular and noncircular geometries using sophisticated computational aerodynamic predictive tools to determine the potential aerodynamic benefits.

The geometry of the baseline circular cross-section geometry is shown in Figure 1. The geometry consists of a conical nose/cylinder/boattail/tail boom/fin assembly which approximates the geometric characteristics of modern CE-type munitions. Two noncircular cross-section geometries have also been considered. These noncircular bodies share similar geometric characteristics with the circular cross-section geometry. The noncircular cross-section geometries were obtained by extruding the baseline circular cross-section geometry through a square cross section of width 43 mm and 50 mm, respectively. A schematic of the circular and two noncircular cross sections is shown in Figure 2. The 43-mm geometry results in a nearly square cross section over the cylindrical portion of the body, while the 50-mm geometry results in a square cross section with rounded corners. Both noncircular cross-section geometries have circular cross sections on the conical nose and on the boattail when the local diameter of the cross section is less than 43 mm and 50 mm, respectively.



ALL DIMENSIONS IN CALIBERS (ONE CALIBER = 120 mm)

Figure 1. Schematic illustration of the baseline circular cross-section flight body.

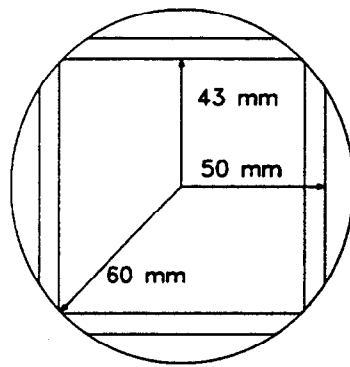


Figure 2. Schematic illustration of the noncircular cross-section geometries.

A fixed fin planform is utilized for all configurations. The fins are oriented in an x-configuration with respect to the noncircular cross-section geometries. This allows the fins to have maximum span without interfering with the walls of the bore. The fin geometry chosen here represents only one option for fin stabilization. It may be possible to utilize folding fins which have a larger span than the bore cross section when deployed in free flight. Nevertheless, the results presented here using the non-folding fins should provide a good basis for evaluating the effects of the noncircular cross section on the aerodynamics of the projectile.

Two additional circular cross-section bodies were considered for the purpose of comparisons. These bodies have the same cross-sectional area as each of the two noncircular cross-section bodies at each axial station along the body. As a result, the bodies have the same total volume as the corresponding noncircular cross-section bodies. For all the geometries considered, the same tail boom and fin assembly were used.

The current study assumes that a functional armature could be built for the geometry under consideration, perhaps a discarding pusher-type armature which might be located between the boattail and the fins. Obviously, for an optimal design, the subprojectile and armature design must be considered simultaneously. This also implies that the characteristics of the gun are defined as well. However, the focus of the current investigation is on the effect of the noncircular cross section on the aerodynamic performance of the flight body. This study should be viewed as a first step for considering the viability of noncircular cross-section geometries for EM gun applications, thereby justifying assumptions regarding the launchability of the geometry under consideration.

2. Computational Approach

Computation of the viscous flow field about the various projectile configurations was accomplished by solving the thin-layer Navier-Stokes equations using the parabolized Navier-Stokes (PNS) technique of Schiff and Steger [1]. Using the PNS technique, computational results were obtained by marching through the grid from the projectile nose to the trailing edge of the fins. This technique is applicable in the supersonic flow regime and requires that the flow field contain no regions of flow separation in the axial direction. Because the computational approach requires only a single sweep through the computational grid, it is very efficient compared with time-marching approaches that require many sweeps through the grid. The technique has been applied successfully to a number of projectile configurations, including axisymmetric shell [2, 3], flared projectiles [4], and finned projectiles [3]. The technique has also been applied previously to predict the aerodynamic performance of a railgun-launched noncircular cross-section projectile [5].

As is standard practice, prediction of the static aerodynamic coefficients such as drag, pitching moment, and normal force coefficients are performed by computing the flow field about the projectile at a fixed angle of attack. Assuming a time-invariant flow field, the steady thin-layer Navier-Stokes equations are applied as shown in equation 1:

$$\frac{\partial \hat{E}}{\partial \xi} + \frac{\partial \hat{F}}{\partial \eta} + \frac{\partial \hat{G}}{\partial \zeta} = \frac{1}{\text{Re}} \frac{\partial \hat{S}}{\partial \zeta}. \quad (1)$$

The thin-layer Navier-Stokes equations are obtained by eliminating from the full Navier-Stokes equations, all the viscous terms except for those containing derivatives in the direction nearly normal to the projectile body. For high Reynolds number flows with no axial flow separation, the thin-layer Navier

Stokes equations are very good approximation to the full Navier-Stokes equations, and can be efficiently solved using available numerical algorithms.

Here, \hat{E} , \hat{F} , and \hat{G} are the inviscid flux vectors, and \hat{S} is the viscous flux vector. Each of these matrices are functions of the dependent variables represented by the vector $q(\rho, \rho u, \rho v, \rho w, e)$, where ρ and e are the density and the total energy per unit volume, and u , v and w , are the velocity components in x , y , and z directions.

The pressure, p , which appears in the flux terms, can be related to the dependent variables by applying the ideal gas law:

$$p = (\gamma - 1) \left[e - \frac{\rho}{2} (u^2 + v^2 + w^2) \right]. \quad (2)$$

A turbulent boundary layer has been simulated over the projectile body using the turbulence model of Baldwin and Lomax [6].

The thin-layer equations are solved using the PNS technique of Schiff and Steger [1]. Following the approach of Schiff and Steger, the governing equations are solved using a conservative, approximately factored, implicit finite-difference numerical algorithm as formulated by Beam and Warming [7]. The computations presented here were performed using a shock-fitting procedure reported by Rai and Chaussee [8]. This procedure solves the five Rankine-Hugoniot jump conditions, two geometric shock-propagation conditions, and one compatibility equation to determine the values of the five dependent variables immediately behind the shock, as well as the position of the shock.

For the computational results presented here, the grid consisted of 60 points from the body to the shock. On the forebody, 72 grid points were utilized around the body in the circumferential direction. To capture the details of the fin geometry, 280 grid points were used in the circumferential direction.

In the marching (axial) direction, 470 marching planes were required for each caliber of body length. Over the axisymmetric portion of the body, the grid was generated algebraically. On the non-conical portion and finned portion of the body, the grid was obtained using an elliptic grid generator [9]. A complete computation for each configuration required approximately 2 hr of computer processor unit (CPU) time on a Cray C-90 supercomputer.

3. Results

Predictions of the aerodynamic performance of the flight bodies were made at flight velocity of Mach 3 at standard atmospheric launch conditions (ambient

temperature of 70 °F). A constant wall temperature of 70 °F on the body surface was used in all the simulations. A constant angle of attack of 2° was used to generate the transverse forces and moments.

3.1 Aerodynamics of the Baseline Circular Cross-Section Geometry

Each of the geometries considered here have similar aerodynamic characteristics. Before comparing the aerodynamic performance of each of the designs, it is useful to examine the aerodynamic characteristics of the baseline circular cross-section configuration.

Figure 3 shows the development of the drag over the baseline configuration. Most the aerodynamic drag is produced by the wave drag on the conical nose of the vehicle. The boattail also produced a significant amount of drag due to the low pressure produced by the flow expansion on the boattail. The amount of drag from the nose and boattail is dependent, in part, on the cross-sectional area, so that reductions in the cross-sectional area may result in improvements in the aerodynamic performance. The skin friction and fin drag account for only a small portion of the total drag. An estimate of the base drag indicates that the expected base drag is about 4% of the forebody drag. The base drag is not included in the plotted drag coefficient data. Computational predictions of the axial force coefficient at 0° and 2° showed less than 1% difference. Because of the small differences in the axial force coefficient at small angles of attack, drag coefficient predictions were obtained using the axial force coefficient from the 2° angle-of-attack solutions for the other body geometries.

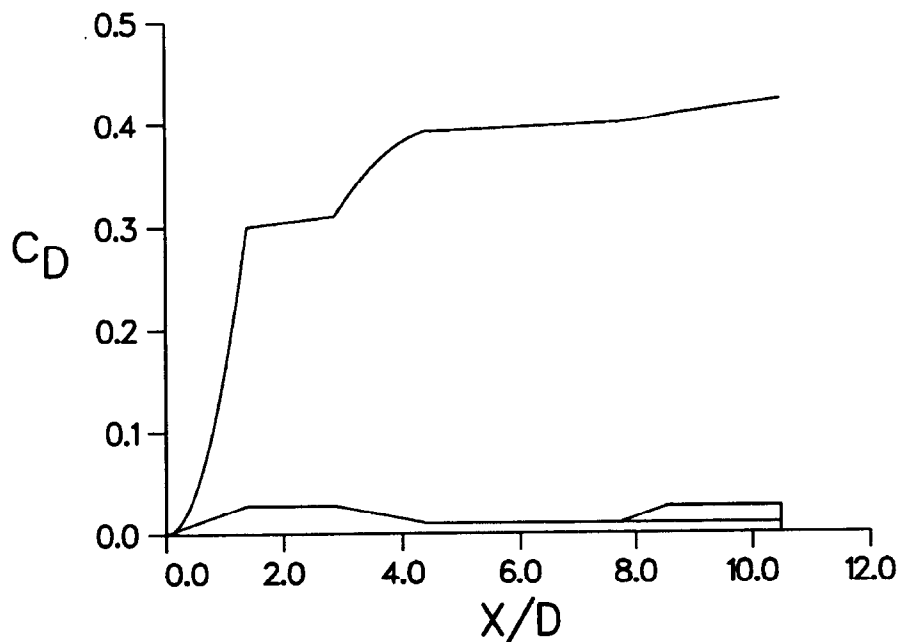


Figure 3. Development of the drag coefficient over the baseline circular cross-section geometry.

CE-type munitions are usually made aerodynamically stable using tail fins. When the projectile is at angle of attack, the tail fins must produce sufficient normal force aft of the projectile's center of gravity to counteract the nose normal force produced in front of the center of gravity. By examining the distribution of the normal force, the relative contribution from each component of the body can be examined. Figure 4 shows the normal force distribution for the circular cross-section geometry. The conical nose and cylindrical portion of the body produce significant amounts of lift on the forward portion of the body. Some of this lift is lost over the boattail. The stabilizing fins produce a significant amount of lift which is required to balance the nose lift in order to maintain aerodynamic stability.

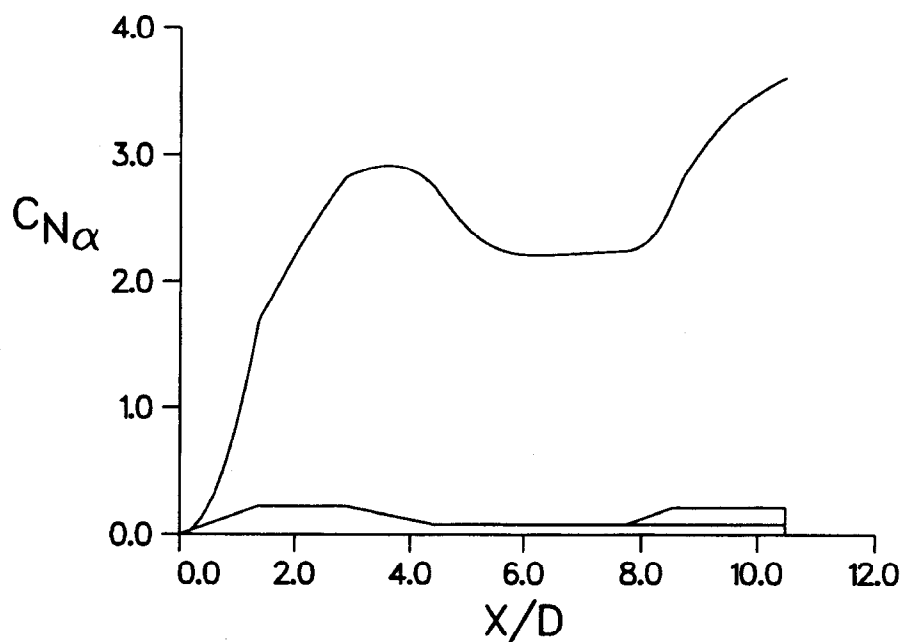


Figure 4. Development of the normal force coefficient over the baseline circular cross-section geometry.

The balance between the lift produced by all the body components is reflected in the pitching moment about the center of gravity of the body. A negative pitching moment coefficient is required for aerodynamic stability and indicates that the fin lift provides sufficient moment to offset the moment produced by the nose lift. Figure 5 shows the distribution of the pitching moment coefficient over the baseline circular cross-section geometry. The conical nose and the cylinder produce a destabilizing moment due to lift in front of the center of gravity. The boattail also provides a destabilizing moment by producing negative lift aft of the center of gravity. The tail fins produce sufficient lift to offset the destabilizing moment from the front of the body, resulting in aerodynamic

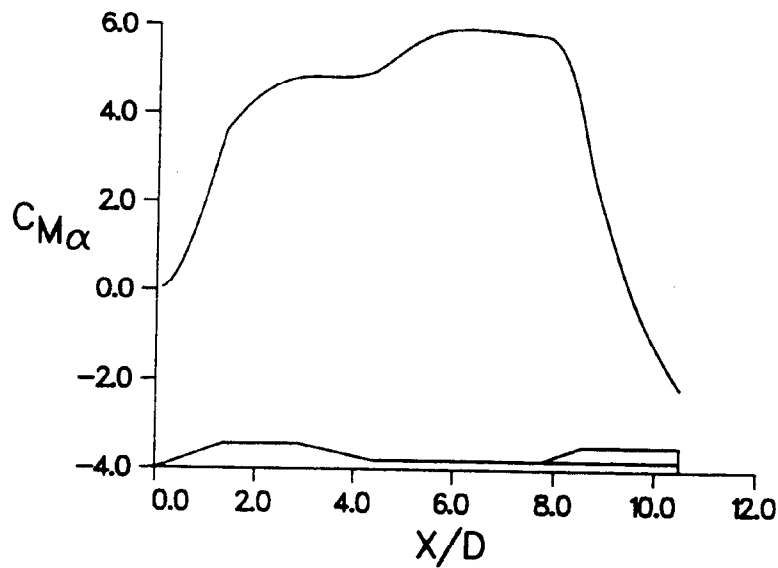


Figure 5. Development of the pitching moment coefficient over the baseline circular cross-section geometry.

stability for the complete configuration. The level of aerodynamic stability is comparable to conventional CE munitions.

3.2 Comparison of Aerodynamics Between Circular and Noncircular Geometries

The effect of noncircular cross sections on aerodynamic performance was examined by comparing the performance of the two noncircular cross-section geometries with the performance of the baseline configuration. Two additional circular cross sections that had the same local cross-sectional area as the nonconical geometries were also considered.

Figure 6 shows the development of the drag coefficient over the baseline circular cross-section body and the two noncircular cross-section bodies. The circular cross-section geometry has the highest drag because of its large frontal area. The two noncircular cross-section geometries show progressively reduced drag as the frontal area is reduced. The drag reduction occurs primarily on the conical nose with some additional drag reduction on the boattailed portion of the body. The tail boom and fin assembly for all three bodies produce nearly identical contributions to the drag of the vehicle.

Figure 7 shows a comparison of the drag for the noncircular cross-section geometries with circular cross-section geometries that possess the same local cross-sectional areas. In each case, the drag for the noncircular cross-section

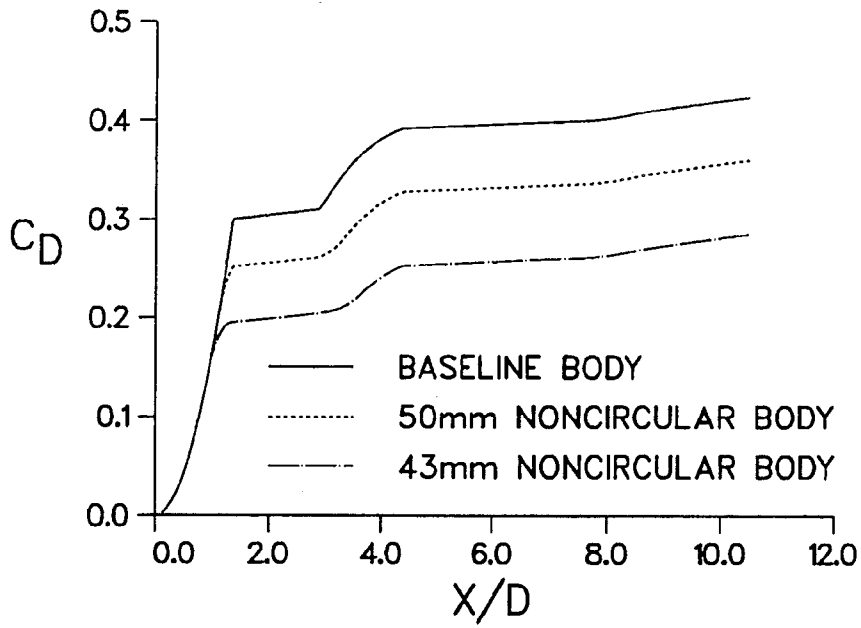


Figure 6. Development of the drag coefficient over the baseline circular cross-section and noncircular cross-section geometries.

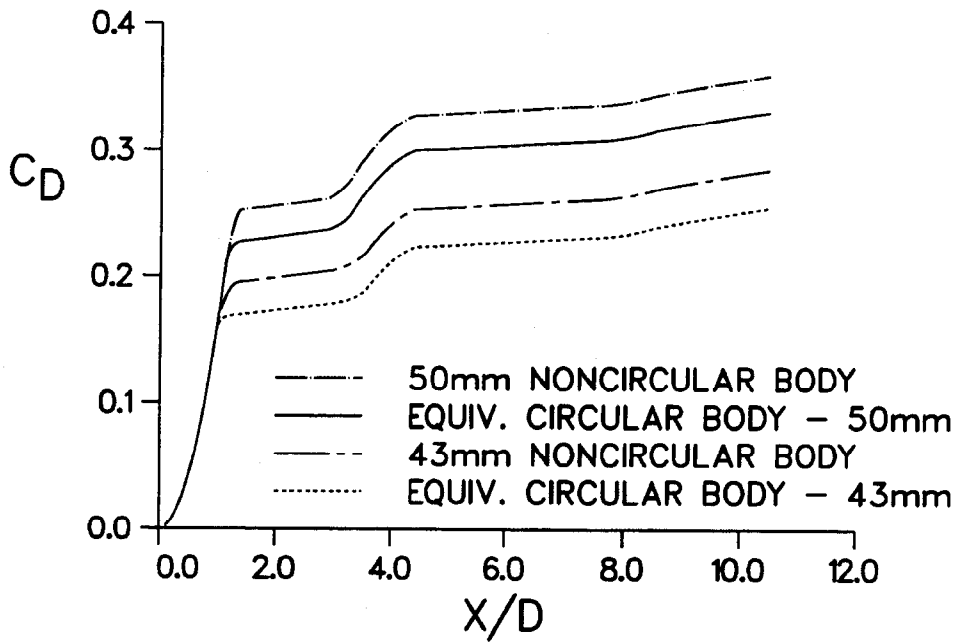


Figure 7. Development of the drag coefficient over the noncircular cross-section geometries and equivalent cross-sectional area circular geometries.

body is greater than the corresponding circular cross-section geometry with the same local cross-sectional geometry. The drag increase occurs primarily on the conical nose with slight increase in drag on the boattailed portion of the body. The results seem to imply that if the payload is a fixed volume whose geometric shape is not constrained, such as high explosive, the configuration exhibiting the lowest drag will be a circular cross-section body. However, payloads with a noncircular cross-sectional geometry, such as an EFP warhead, may be effectively packaged in a noncircular cross-section flight body to yield improved drag performance relative to circular cross-sectional geometries. Most of the drag saving will result from the reduction of cross-sectional area on the nose of the flight body.

The results for the three circular cross-section geometries show that as the cross-sectional area of the nose is reduced, the pitching moment coefficient becomes increasingly more negative yielding more stability for the configuration, as shown in Figure 8. Most of the increased stability is due to the reductions in the nose lift produced by the reduced cross-sectional area of the nose, as shown in Figure 9. The configurations with the smaller cross-sectional area show a small increase in the stabilizing moment from the fins, which are presumably due to the reduction in the wake from the nose that interacts with the fins to reduce their effectiveness.

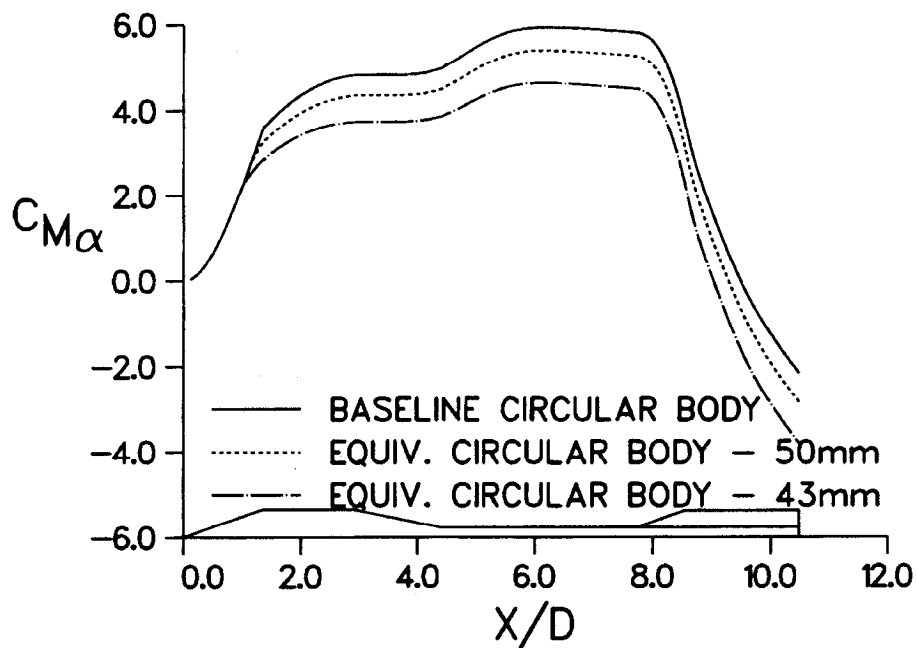


Figure 8. Development of the pitching moment coefficient over the circular cross-section geometries.

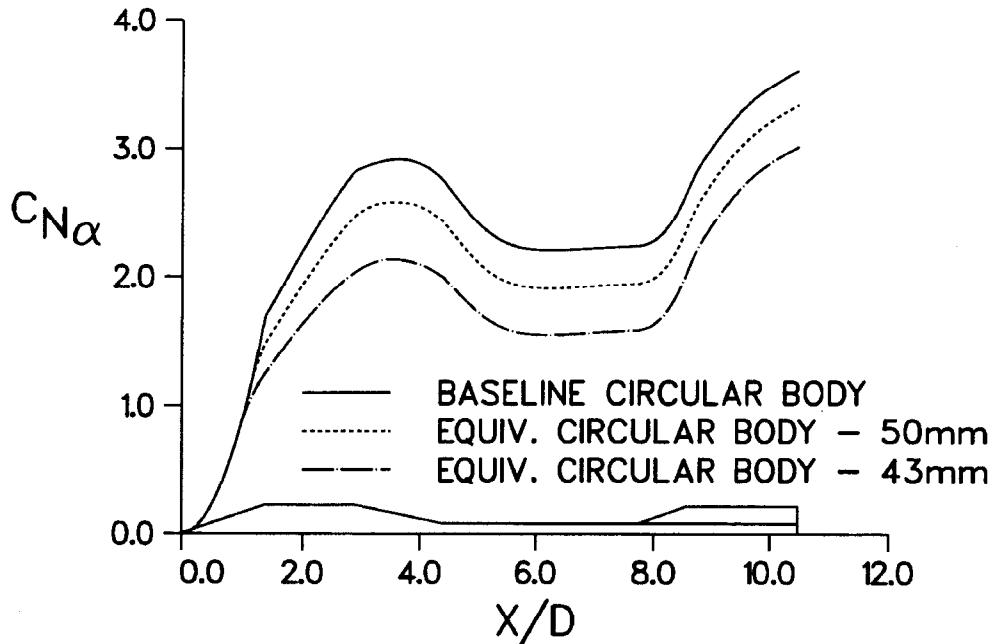


Figure 9. Development of the normal force coefficient over the circular cross-section geometries.

The relative stability of the baseline circular cross-sectional geometry and the noncircular cross-section geometries is compared in Figures 10 and 11. The results show that as the cross-sectional geometry of the nose is reduced, the moment contribution from the nose lift is reduced yielding more stability. This is a similar trend as that observed for the circular cross-section geometries. However, the moment contribution from the fins appears to be significantly affected by the noncircular cross section of the nose. The circular cross-section geometry produces a more stabilizing moment from the fin than the noncircular geometries with the square cross-section geometry producing the least stabilizing moment. This appears to be due to an interaction of crossflow separation vortices produced at the corners of the noncircular cross section with the fins. Figures 12 and 13 show crossflow particle traces at an axial station 7.5 cal. from the nose and immediately in front of the fins for the circular and 43-mm noncircular cross-section bodies, respectively. The crossflow particle traces show the presence of two lee-side crossflow vortices for the circular cross-section body (Figure 12). Lee-side crossflow vortices are fairly common on slender flight vehicles and produced by a crossflow separation from the crossflow wake. The noncircular cross-section body also has two lee-side vortices as well as two vortices on the windside of the body (Figure 13).

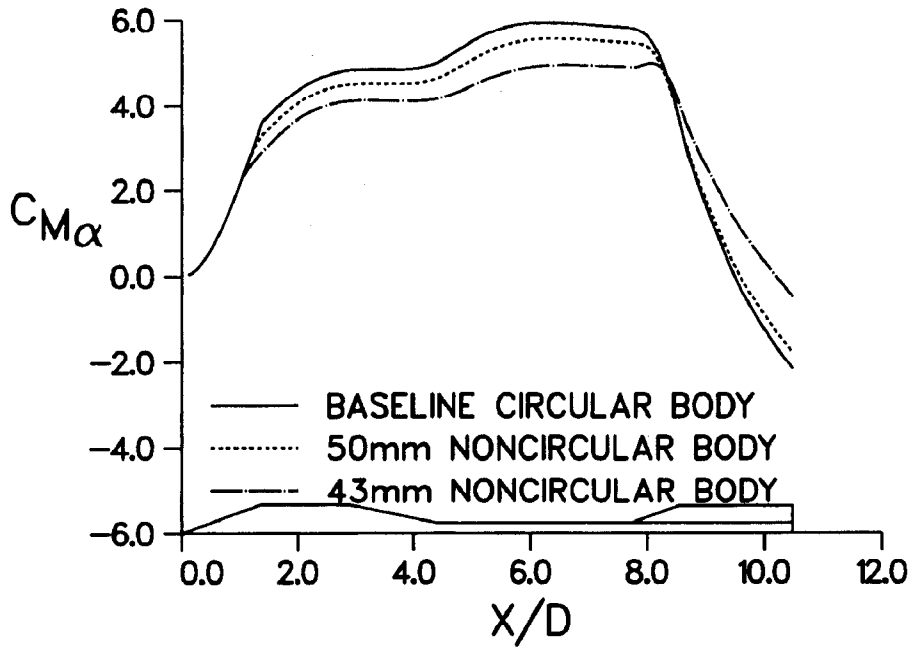


Figure 10. Development of the pitching moment coefficient over the baseline circular cross-section and noncircular cross-section geometries.

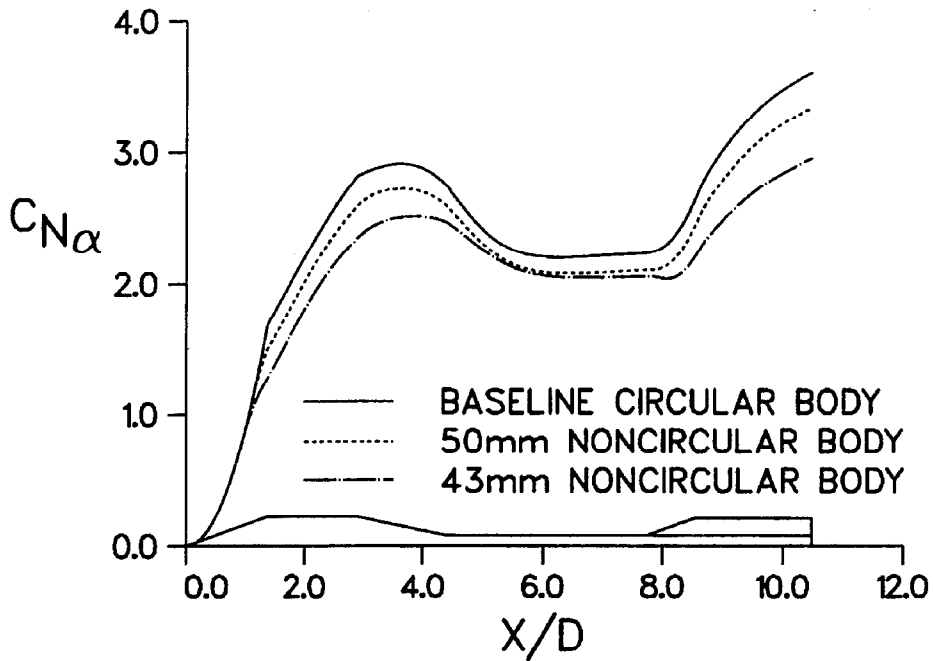


Figure 11. Development of the normal force coefficient over the baseline circular cross-section and noncircular cross-section geometries.

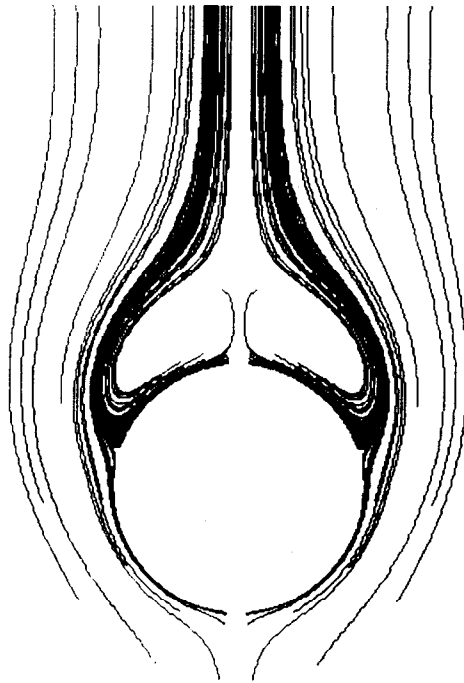


Figure 12. Crossflow particle traces at $X/D=7.5$, circular cross-section body, Mach 3, 2° angle of attack.

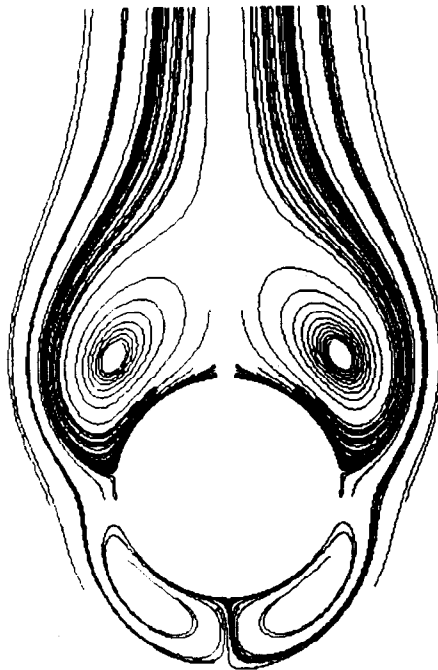


Figure 13. Crossflow particle traces at $X/D=7.5$, 43-mm noncircular cross-section body, Mach 3, 2° angle of attack.

3.3 Effect of Roll Orientation on Aerodynamic Performance

For completely axisymmetric bodies, the aerodynamic performance of the flight body will be independent of roll orientation. (This behavior is limited to small-to-moderate angles of attack where the lee-side vortices are symmetric.) For noncircular cross sections, the aerodynamics may exhibit some dependence on roll orientation. If the body's roll rate is above the pitching frequency, the effect of roll orientation is often averaged out. If the body is not rolling, the effect of roll orientation on the aerodynamics may be more important. Computations were performed to assess the effect of roll orientation. The computations presented previously were performed with the body oriented in the "x orientation" with respect to the pitch plane. In other words, the pitch plane was oriented between the fins and the corners of the noncircular cross section. Additional computations were performed with the body rolled at 22.5° and 45° from the x orientation. The 45° roll orientation is often referred to as the "+ orientation" since the fins and corners aligned with the pitch plane.

The baseline circular cross-section body showed some roll orientation dependence in the normal force and pitching moment over the finned portion of the body as shown in Figures 14 and 15. This is not completely unexpected since the fin lift should be affected by the orientation of the fins with respect to the lee-side vortices. With the fins oriented in the + orientation, the horizontal (lift producing) fins are below the lee-side vortices. In the x orientation, the two lee-side fins are located within the lee-side vortices. As a result, the normal force coefficient increases by 3.4% compared with the x orientation. Because of the long moment arm from the center of gravity (CG) to the fins, the pitching moment increases by approximately 30%.

The normal force and pitching moment coefficients for the noncircular cross-section body displays dependence on roll angle over both the forebody and the fins as shown in Figures 16 and 17. It is interesting to note that the roll dependence in the transverse force and moment on the forebody occurs downstream of the noncircular cross section, rather than on the portion of the body with the noncircular cross section. This is likely due to differences in the wake and vortex patterns between the various roll orientations. The variation of the normal force and pitching moment coefficient with roll angle is actually less than that of the baseline circular cross-section body.

The simulations showed very little effect of roll orientation on the axial force at 2° angle of attack (less than 0.2%) for either the baseline circular cross-section body or the 43-mm noncircular cross-section body.

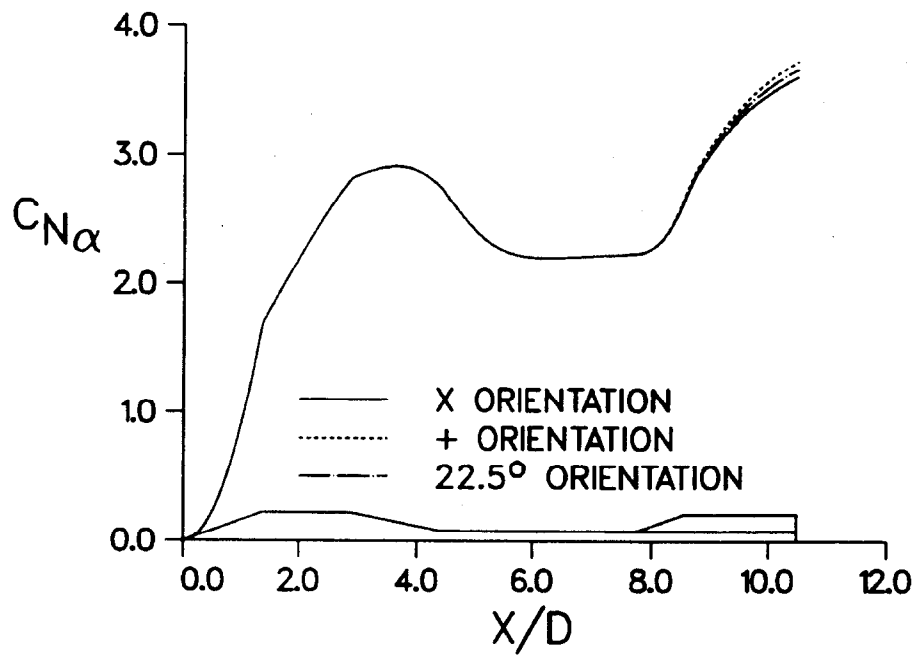


Figure 14. Effect of roll orientation on the development of the normal force coefficient over the baseline circular cross-section geometry.

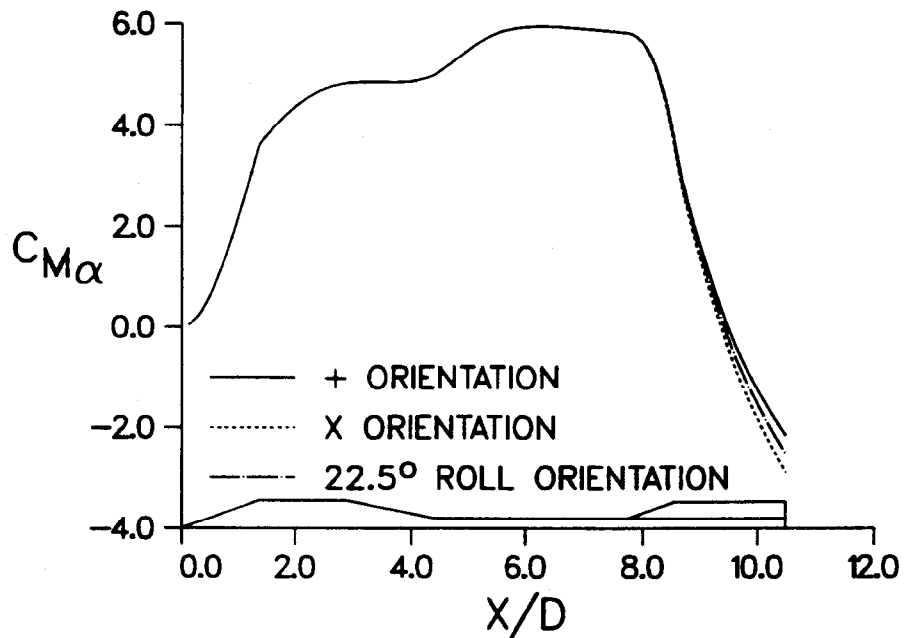


Figure 15. Effect of roll orientation on the development of the pitching moment coefficient over the baseline circular cross-section geometry.

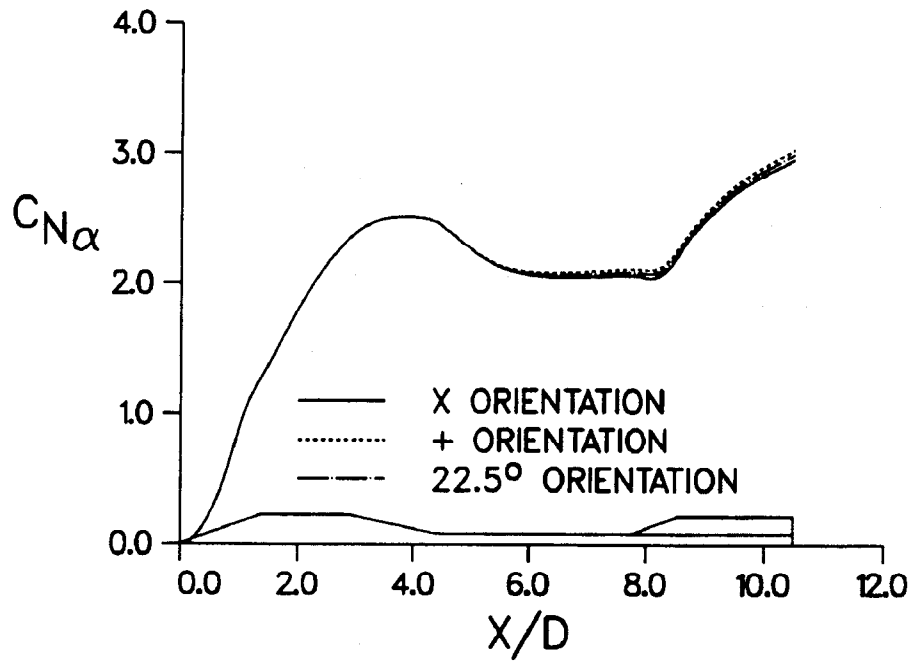


Figure 16. Effect of roll orientation on the development of the normal force coefficient over the 43-mm noncircular cross-section geometry.

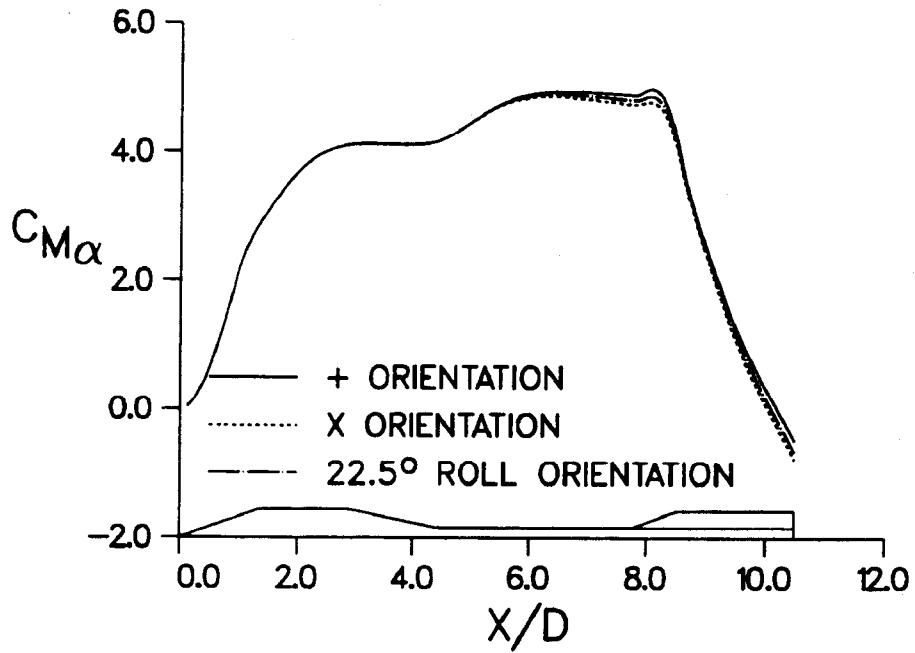


Figure 17. Effect of roll orientation on the development of the pitching moment coefficient over the baseline circular cross-section geometry.

4. Conclusion

The study presented here demonstrates the potential for aerodynamic benefits of noncircular cross-section bodies when compared with circular cross-section bodies. The results show that significant reduction in drag is possible through the use of a noncircular cross section under certain constraints. In particular, if the geometric constraints of the payload conform more readily to a noncircular cross-section body, there is a potential for aerodynamic benefits such as improved stability and drag reduction. If the payload is not geometrically constrained and can fit in a fixed volume, the results indicate that a circular cross section provides optimal aerodynamic performance.

For the particular configurations examined here, the transverse aerodynamic force and moments for the noncircular cross-section bodies did not display a significant dependence on roll orientation. In fact, the roll dependence produced by the roll orientation of fins produced a more significant effect than the roll orientation effects of the noncircular body cross section.

Finally, this particular study was performed using sophisticated computational tools. The results indicate that some of the aerodynamic effects demonstrated here can be predicted using simpler aerodynamic models although others cannot. Thus the use of sophisticated tools, even in preliminary or conceptual aerodynamic design, may be justified, particularly when the configurations of interest are sufficiently different than those of typical interest.

5. References

1. Schiff, L. B., and J. L. Steger. "Numerical Simulation of Steady Supersonic Viscous Flow." *AIAA Journal*, vol. 18, no. 12, pp. 1421-1430, December 1980.
2. Sturek, W. B., D. C. Mylin, B. J. Guidos, and C. J. Nietubicz. "Navier-Stokes Computational Study of the Influence of Shell Geometry on the Magnus Effect at Supersonic Speeds." BRL-TR-2501, U.S. Army Ballistic Research Laboratory, Aberdeen Proving Ground, MD, June 1983.
3. Weinacht, P., B. J. Guidos, L. D. Kayser, and W. B. Sturek. "PNS Computations for Spinning and Fin-Stabilized Projectiles at Supersonic Velocities." BRL-MR-3464, U.S. Army Ballistic Research Laboratory, Aberdeen Proving Ground, MD, September 1985.
4. Danberg, J. E., A. Sigal, and I. Celmins. "Prediction and Comparison With Measurements of the Aerodynamic Characteristics of Flare-Stabilized XM910 Prototypes." BRL-MR-3752, U.S. Army Ballistic Research Laboratory, Aberdeen Proving Ground, MD, May 1989.
5. Weinacht, P. "Application of Computational Fluid Dynamics to the Analysis of the Aerodynamics of a Railgun Projectile." BRL-MR-3742, U.S. Army Ballistic Research Laboratory, Aberdeen Proving Ground, MD, March 1989.
6. Baldwin, B. S., and H. Lomax. "Thin Layer Approximation and Algebraic Model for Separated Turbulent Flows." AIAA Paper 78-257, AIAA 16th Aerospace Sciences Meeting, Huntsville, AL, January 1978.
7. Beam, R., and R. F. Warming. "An Implicit Factored Scheme for the Compressible Navier-Stokes Equations." *AIAA Journal*, vol. 16, no. 4, pp. 393-402, 1978.
8. Rai, M. M., and D. S. Chaussee. "New Implicit Boundary Procedure: Theory and Applications." AIAA Paper 83-0123, AIAA 23rd Aerospace Sciences Meeting, Reno, NV, January 1983.
9. Rai, M. M., Chaussee, D. S., and Rizk, Y. M. "Calculation of Viscous Supersonic Flows Over Finned Bodies." AIAA Paper 83-1667, July 1983.

INTENTIONALLY LEFT BLANK.

<u>NO. OF COPIES</u>	<u>ORGANIZATION</u>	<u>NO. OF COPIES</u>	<u>ORGANIZATION</u>
2	DEFENSE TECHNICAL INFORMATION CENTER DTIC DDA 8725 JOHN J KINGMAN RD STE 0944 FT BELVOIR VA 22060-6218	1	DIRECTOR US ARMY RESEARCH LAB AMSRL D D R SMITH 2800 POWDER MILL RD ADELPHI MD 20783-1197
1	HQDA DAMO FDT 400 ARMY PENTAGON WASHINGTON DC 20310-0460	1	DIRECTOR US ARMY RESEARCH LAB AMSRL DD 2800 POWDER MILL RD ADELPHI MD 20783-1197
1	OSD OUSD(A&T)/ODDDR&E(R) R J TREW THE PENTAGON WASHINGTON DC 20301-7100	1	DIRECTOR US ARMY RESEARCH LAB AMSRL CI AI R (RECORDS MGMT) 2800 POWDER MILL RD ADELPHI MD 20783-1145
1	DPTY CG FOR RDA US ARMY MATERIEL CMD AMCRDA 5001 EISENHOWER AVE ALEXANDRIA VA 22333-0001	3	DIRECTOR US ARMY RESEARCH LAB AMSRL CI LL 2800 POWDER MILL RD ADELPHI MD 20783-1145
1	INST FOR ADVNCD TCHNLGY THE UNIV OF TEXAS AT AUSTIN PO BOX 202797 AUSTIN TX 78720-2797	1	DIRECTOR US ARMY RESEARCH LAB AMSRL CI AP 2800 POWDER MILL RD ADELPHI MD 20783-1197
1	DARPA B KASPAR 3701 N FAIRFAX DR ARLINGTON VA 22203-1714		<u>ABERDEEN PROVING GROUND.</u>
1	US MILITARY ACADEMY MATH SCI CTR OF EXCELLENCE MADN MATH MAJ HUBER THAYER HALL WEST POINT NY 10996-1786	4	DIR USARL AMSRL CI LP (BLDG 305)

<u>NO. OF COPIES</u>	<u>ORGANIZATION</u>	<u>NO. OF COPIES</u>	<u>ORGANIZATION</u>
1	AIR FORCE RESEARCH LABORATORY AFRL/VAA DR J SHANG BLDG 146B 2210 8TH ST WPAFB OH 45433-7510	1	COMMANDER USAAMCOM AMSAM RS SS G LANDINGHAM REDSTONE ARSENAL AL 35898-5252
2	AIR FORCE RESEARCH LABORATORY AFRL/MNAV G ABATE G WINCHENBACH 101 W EGLIN BLVD STE 219 EGLIN AFB FL 32542-6810	2	COMMANDER USAAMCOM AMSAM RD SS AS E VAUGHN D WASHINGTON REDSTONE ARSENAL AL 35898-5252
1	COMMANDER NSWC WEAPONS SYS DEPT G04 17320 DAHLGREN RD DR F MOORE DAHLGREN VA 22448-5150	1	COMMANDER NSWC CODE 420 DR A WARDLAW INDIAN HEAD MD 20640-5035
1	COMMANDER NSWC WEAPONS SYS DEPT G04 17320 DAHLGREN RD T HYMER DAHLGREN VA 22448-5150	1	MIT TECH LIBRARY 77 MASSACHUSETTES AVE CAMBRIDGE MA 02139
1	THE UNIVERSITY OF TEXAS AT AUSTIN INSTITUTE FOR ADVANCED TECHNOLOGY DR W REINECKE 4030 2 W BRAKER LN AUSTIN TX 78759-5329	1	MISSISSIPPI STATE UNIV ENG RES CNTR RM 228 PROF B SONI BOX 9627 MS STATE MS 39762
4	COMMANDER US ARMY TACOM ARDEC AMSTE AR FSF T C NG H HUDGINS B WONG J GRAU BLDG 382 PICATINNY ARSENAL NJ 07806-5000	1	UNIVERSITY OF TEXAS DEPT OF MECH ENGRNG DR D S DOLLING AUSTIN TX 78712-1085
		2	LOCKHEED MARTIN VOUGHT SYS DEPT OF MECH ENGRNG P A WOODEN W B BROOKS PO BOX 65003 MS ME 55 DALLAS TX 75265-0003

<u>NO. OF COPIES</u>	<u>ORGANIZATION</u>	<u>NO. OF COPIES</u>	<u>ORGANIZATION</u>
2	ARROW TECH ASSOCIATES R WHYTE W HATHAWAY 1233 SHELBURNE RD STE D8 SOUTH BURLINGTON VT 05403	1	US ARMY TACOM ARDEC FSAE GCSS TMA J BENNETT BLDG 354 PICATINNY ARSENAL NJ 07806-5000
1	OREGON STATE UNIV DEPT MECH ENGRNG DR M COSTELLO CORVALLIS OR 97331	3	THE UNIVERSITY OF TEXAS AT AUSTIN INSTITUTE FOR ADVANCED TECHNOLOGY P SULLIVAN F STEPHANI T WATT 4030 2 W BRAKER LN AUSTIN TX 78759-5329
1	UNIV OF ILLINOIS AT URBANA CHAMPAIGN DEPT OF MECH AND INDUSTRIAL ENGRNG DR J C DUTTON URBANA IL 61801	4	UNIV OF TEXAS AT AUSTIN CENTER OF ELECTROMAGNETICS A WALL J KITZMILLER S PRATAP J PAPPAS AUSTIN TX 78712
1	METACOMP TECHNOLOGIES INC S R CHAKRAVARTHY 650 HAMPSHIRE RD STE 200 WESTLAKE VILLAGE CA 91361-2510	2	LOCKHEED MARTIN VOUGHT L FARRIS K COOK PO BOX 650003 MS WT 21 DALLAS TX 75265-0003
1	LAWRENCE LIVERMORE NATL LAB DR M J GRAHAM PO BOX 808 LIVERMORE CA 94550	1	INST FOR DEFENSE ANALYSIS I KOHLBERG 1801 N BEAUREGARD ST ALEXANDRIA VA 22311
1	TETRA RESEARCH CORP DR R CHAMBERLAIN 2610 SPICEWOOD TR HUNTSVILLE AL 35811-2604	1	KAMEN ELECTROMAGNETICS CORP P MONGEAU 2 FOX RD HUDSON MA 01749
1	DIR FOR THE DIRECTORATE OF FORCE DEVELOPMENT US ARMY ARMOR CTR COL E BRYLA FT KNOX KY 40121-5000		
2	US ARMY TACOM TARDEC AMSTA TR D J CHAPIN M TOURNER MS 207 WARREN MI 48397-5000		

<u>NO. OF COPIES</u>	<u>ORGANIZATION</u>
1	SUNY AT BUFFALO J SARGEANT PO BOX 601900 BUFFALO NY 14260-1900
1	SAIC J BATTEH 4901 OLDE TOWNE PKWY STE 200 MARIETTA GA 30068
2	UDLP B GOODEL R JOHNSON MS M170 4800 EAST RIVER RD MINNEAPOLIS MN 55421-1498
1	UNIV OF TEXAS AT AUSTIN M DRIGA ENS 434 DEPT OF ECE MAIL CODE 60803 AUSTIN TX 78712
1	SAIC G CHRYSSOMALLIS 3800 WEST 80TH ST STE 1090 BLOOMINGTON MN 55431
1	SAIC K A JAMISON 1247B N EGLIN PKWY SHALIMAR FL 32579
2	IAP RESEARCH INC D BAUER J BARBER 2763 CULVER AVE DAYTON OH 45429-3723
2	MAXWELL TECHNOLOGIES P REIDY T WOLFE 9244 BALBOA AVE SAN DIEGO CA 92123

<u>NO. OF COPIES</u>	<u>ORGANIZATION</u>
1	NORTH CAROLINA STATE UNIV M BOURHAM DEPT OF NUCLEAR ENGR BOX 7909 RALEIGH NC 27695-7909
1	MAXWELL PHYSICS INTERNATIONAL C GILMAN 2700 MERCED ST PO BOX 5010 SAN LEANDRO CA 94577-0599
1	ATA ASSOCIATES W ISBELL PO BOX 6570 SANTA BARBARA CA 93160-6570

ABERDEEN PROVING GROUND

3	CDR US ARMY ARDEC FIRING TABLES BRANCH R LIESKE R EITMILLER F MIRABELLE BLDG 120 APG MD 21005
31	DIR USARL AMSRL WM E M SCHMIDT D SMITH AMSRL WM B A W HORST JR W CIPEIELLA AMSRL WM BA D LYON F BRANDON T BROWN AMSRL WM BD B FORCH M NUSCA AMSRL WM BF J LACETERA

NO. OF
COPIES ORGANIZATION

ABERDEEN PROVING GROUND (CONT)

AMSRL CI H
C NIETUBICZ
W STUREK
AMSRL CI HA
R NOACK
AMSRL WM BC
P PLOSTINS
M BUNDY
G COOPER
M DELGUERCIO
J DESPIRITO
T ERLINE
J GARNER
B GUIDOS
K HEAVEY
J NEWILL
V OSKAY
J SAHU
K SOENCKSEN
D WEBB
P WEINACHT (3 CPS)
A ZIELINSKI

INTENTIONALLY LEFT BLANK.

REPORT DOCUMENTATION PAGE

Form Approved
OMB No. 0704-0188

Public reporting burden for this collection of information is estimated to average 1 hour per response, including the time for reviewing instructions, searching existing data sources, gathering and maintaining the data needed, and completing and reviewing the collection of information. Send comments regarding this burden estimate or any other aspect of this collection of information, including suggestions for reducing this burden, to Washington Headquarters Services, Directorate for Information Operations and Reports, 1215 Jefferson Davis Highway, Suite 1204, Arlington, VA 22202-4302, and to the Office of Management and Budget, Paperwork Reduction Project(0704-0188), Washington, DC 20503.

1. AGENCY USE ONLY (Leave blank)	2. REPORT DATE <p style="text-align: center;">April 2001</p>	3. REPORT TYPE AND DATES COVERED <p style="text-align: center;">Final, 1 October 1996-31 September 1997</p>
4. TITLE AND SUBTITLE Effect of Body Cross Section on Projectile Aerodynamic Performance With Application to Electromagnetic (EM) Guns		5. FUNDING NUMBERS ILI612618AH80
6. AUTHOR(S) Paul Weinacht		
7. PERFORMING ORGANIZATION NAME(S) AND ADDRESS(ES) U.S. Army Research Laboratory ATTN: AMSRL-WM-BC Aberdeen Proving Ground, MD 21005-5066		8. PERFORMING ORGANIZATION REPORT NUMBER ARL-TR-2445
9. SPONSORING/MONITORING AGENCY NAMES(S) AND ADDRESS(ES)		10. SPONSORING/MONITORING AGENCY REPORT NUMBER
11. SUPPLEMENTARY NOTES		
12a. DISTRIBUTION/AVAILABILITY STATEMENT Approved for public release; distribution is unlimited.		12b. DISTRIBUTION CODE
13. ABSTRACT (Maximum 200 words) <p>The most effective bore cross-section geometry for electromagnetic (EM) guns may differ significantly from the circular cross section of conventional guns. The geometry of the bore cross section will influence the shape of the armature/subprojectile launch package. For certain applications, a noncircular cross section may provide payload packaging benefits which have not been considered previously for conventional circular cross-section guns. Whether these benefits can be fully realized depends, in part, on the aerodynamic performance of these geometries in free flight. The current study considers the aerodynamics of chemical energy (CE)-type munitions to determine whether there are potential aerodynamic benefits for noncircular cross-section geometries compared with conventional circular cross-section bodies. The study compares the aerodynamic drag and static stability of both circular and noncircular geometries using sophisticated computational aerodynamic predictive tools to determine the potential aerodynamic benefits.</p>		
14. SUBJECT TERMS projectile aerodynamics, EM guns, computational fluid dynamics		15. NUMBER OF PAGES <p style="text-align: center;">27</p>
		16. PRICE CODE
17. SECURITY CLASSIFICATION OF REPORT <p style="text-align: center;">UNCLASSIFIED</p>	18. SECURITY CLASSIFICATION OF THIS PAGE <p style="text-align: center;">UNCLASSIFIED</p>	19. SECURITY CLASSIFICATION OF ABSTRACT <p style="text-align: center;">UNCLASSIFIED</p>
20. LIMITATION OF ABSTRACT <p style="text-align: center;">UL</p>		

INTENTIONALLY LEFT BLANK.